Launch Vibration of Pre-Tensioned Coiled Structures

Alexander Wen* and Sergio Pellegrino†
California Institute of Technology, Pasadena, CA, 91125

Relative movement between slipping layers in a coil due to vibration can cause defects in the structure or damage functional elements, such as photovoltaic cells, attached to the structure. Radial contact pressure between successive layers due to coiling pre-tension provides a frictional force that can be used to resist inter-layer slip. In this study, we propose a stress-field based, analytical friction model to use as a criterion for estimating the frictional shear capacity of a wound roll prior to the onset of slip. Because the radial pressure varies with radial position in the coil, the shear capacity against slippage also varies with position. This analytical shear capacity can then be compared against the shear resultants obtained in finite-element simulations of coiled structures undergoing vibration load. Rather than modeling discrete windings of wound rolls, the starting coiled-stiff assumption is the coil is tensioned sufficiently to behave as a solid. Thus, a finite-element vibration study of a homogenized solid is used to find the loads and locations where shear resultant is larger than the estimated shear capacity, indicating slip. The validity of the coiled-stiff assumption is experimentally verified using a vibration experiment that measures the variation in apparent stiffness of a coiled membrane wound under varying tensions.

I. Introduction

Large structures in space have many applications and their functional aperture scales with size. Because rocket fairings are limited in space, structures must be packaged to a reduced size for launch. Coiling is a packaging architecture with high packing efficiency and has seen increased usage for state of the art deployable structures such as IKAROS, ROSA, and Starshade [1–3]. In order to safely deliver these structures to orbit, the coil must withstand launch vibration, which is the main loading of structures during launch. If the structure is insufficiently restrained, vibration loads can cause inter-layer slip in the coil.

Relative movement between coiled layers due to slip can cause defects in the structure or damage any functional elements attached to the structure. A general problem with all coiled structures is the question of how to prevent slip. One approach is to add restraint features, for example, discrete hold down release mechanisms [4, 5]. However, a potential risk with each additional restraint is creating a new single point of failure for deployment. Instead, we propose a scheme that relies on coiling pre-tension to provide integral packing and slip resistance. In general, coils are tightly wound with a pre-tension in order to promote good packing efficiency and prevent coiling defects such as wrinkling, blossoming, and buckling [6]. Now, we propose that the coiling pre-tension is chosen large enough to also support inter-layer friction forces which can resist slip. In this respect, coiling turns the structure into its own support against vibration loading.

For this paper, we consider the structure that undergoes coiling as a continuous sheet or film with homogeneous properties and uniform thickness. This simplification allows us to adapt existing studies performed in the roll winding industry and reduce the complexity of our finite-element models. The load carrying capacity of wound rolls of paper, aluminum, steel, etc, used in ground based applications are studied through the modeling of stress-fields that arise in the coil due to winding. Previous studies of wound rolls have created models for radial stresses at any radial position inside a coil wound around a mandrel at constant pre-tension. These stress models have been validated against experiments using compression tests or pressure gauges for a number of materials [7, 8]. The utility of these models in slip estimating has been demonstrated experimentally using dynamic torsional loads [9]. Furthermore, sufficiently tensioned coils are observed to have measurably reduced slip compared to coils wound with looser tension in response to vibration loads [10]. However, a comprehensive experimentally-verified model to predict the slip resistance of coiled structures under vibration loading is not yet available.

*PhD Candidate, Graduate Aerospace Laboratories, 1200 E. California Blvd, MC105-50, Pasadena. email: awwen@caltech.edu.

†Joyce and Kent Kresa Professor of Aerospace and Professor of Civil Engineering, Graduate Aerospace Laboratories, 1200 E. California Blvd, MC105-50, Pasadena. AIAA Fellow. email: sergiop@caltech.edu.

The objective of this research is to investigate whether a coiled structure may be tensioned sufficiently to resist vibration induced slip. To do this, we first need a model for how coiling pre-tension and the number of windings correspond to the inter-layer stresses that provide the required friction forces. This is done by using a stress-field based, analytical friction model to estimate the frictional shear capacity at any point in the wound roll, given a constant winding pre-stress around a mandrel of known dimension. An estimate of the maximum inter-layer friction forces can then be generated from coiling pre-tension values. Next, the effectiveness of frictional capacity needs to be evaluated by comparison against the shear forces observed under vibration loads. This is used to determine what loads can a tensioned coil support without slip and, for loads where slip is expected, the locations where slip occurs.

We begin with the assumption that the coil has been sufficiently pre-tensioned so that the no-slip occurs, and therefore we assume it behaves as a continuous solid. This coiled-stiffness assumption allows us to perform a finite-element analysis (FEA) using a homogenized solid representation of a coil, as opposed to modeling the individual layers in the coil, which is computationally expensive. For this study, we will use the geometry and properties of a notional structure. The homogenized solid coil is attached to an elastic mandrel and a sinusoidal base excitation is applied, emulating a spacecraft vibration test. The resulting stresses of interest are the shear stresses in the directions that can induce inter-layer slip. If for any point in the coil, the resultant of the shear stresses is below the frictional shear capacity, then no slip can occur and the homogenized solid model may be considered as correct. Conversely, this can also be used to determine at what locations a coil slips when the applied load exceeds the frictional capacity and the solid assumption no longer applies.

Vibration experiments will be performed to demonstrate the validity of the coiled-stiffness assumption. We want to determine whether a sufficiently pre-stressed layered assembly can behave as a solid under vibration. This will be done by comparing the stiffness of a wound roll of continuous films measured experimentally using the fundamental frequency against that of an equivalently sized solid obtained from FEA.

II. Model for quantifying slip resistance

For a thin, continuous sheet of constant thickness, h, and negligible bending stiffness wound around a mandrel of radius, r_m, at constant winding tension, T_w the incremental inter-layer stress, $\delta\sigma_{rr}$, of the i^{th} winding (Fig. 1) can be estimated from [7, 8]:

$$\delta\sigma_{rr} = \left[\frac{T_w}{r_m + (i-1)h}\right] h \tag{1}$$

This formulation assumes the stress field is only a function of radial position, and has no angular or axial dependence.

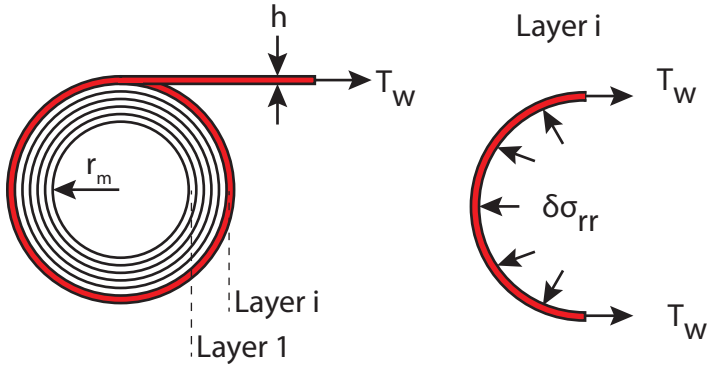

Fig. 1 Winding geometry.

For a known number of windings, this formula can be recursively applied to get a distribution of the inter-layer stress, σ_{rr}, at any point in the coil. Since the additional winding compresses the other layers beneath it, the radial stress field will be maximum at the mandrel interface and tapers outwards for subsequent layers.

The compressive inter-layer stress, σ_{rr}, provides the normal force which is necessary for two surfaces to support a friction force. The maximum stress provided by friction to prevent slip at an interface can be defined as the shear capacity, σ_c, which is proportional to the inter-layer stress through the coefficient of friction μ [9]:

$$\sigma_c = \mu\sigma_{rr} \tag{2}$$

Under loading, the deformation loads for a wound roll correspond to the out-of-plane axial and in-plane tangential shear directions, Fig. 2a. The expected failure modes for axial shear, σ_{rz}, is telescoping, Fig. 2b, while in-plane shear, $\sigma_{r\theta}$, can result in torsion, Fig. 2c. The resultant of the out-of-plane and in-plane shear stresses at a point can be calculated from [11]:

$$\sigma_s = \sqrt{{\sigma_{rz}}^2 + {\sigma_{r\theta}}^2} \tag{3}$$

The shear resultant at any point in the coil can then be compared against the estimated shear capacity at that layer using the criterion:

$$\text{Layer State} = \begin{cases} \text{no-slip} & \text{if } \sigma_c \geq \sigma_s \\ \text{slip} & \text{if } \sigma_c < \sigma_s \end{cases} \tag{4}$$

This criterion can now be used in conjunction with FEA to determine where a coiled structure will slip under vibration loading.

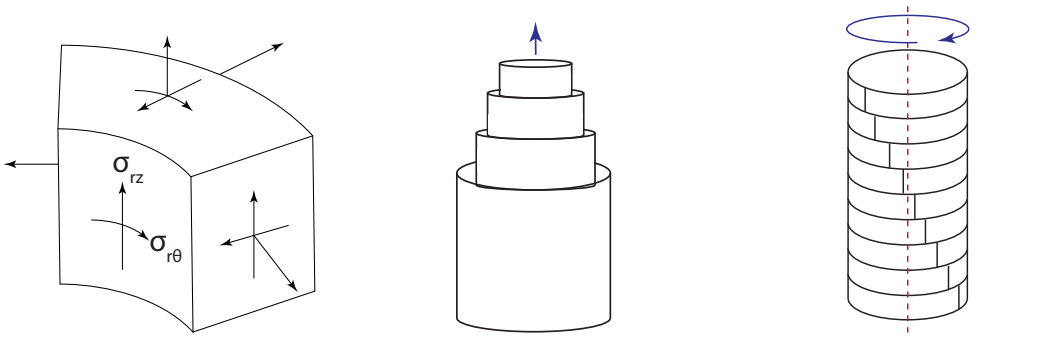

(a) Shear components of interest for interlayer slip

(b) Out of plane defect: telescoping

(c) In plane defect: torsion

Fig. 2 Shear components and associated slip-based defects.

III. Determining locations of slip

We are now interested in applying the shear capacity criterion to determine the performance of frictional resistance concept. Specifically for realistic winding tensions, what vibration loads can the coil support where there is no slip expected? For loading where slip is expected, where does slip initiate? Here we will study the vibration of notional structure with material properties based on a coilable structure being developed at Caltech and geometry informed from scaling the structure to a larger size.

A. Coiled-stiff FEA model properties

Rather than modeling discrete windings of the wound structure, which is computationally expensive, we begin with the assumption that the coil is tensioned sufficiently that no interlayer slip occurs, and it behaves mechanically as a continuous solid. An assumption we will hereafter refer to as the *coiled-stiff* assumption. Thus, our model consists of a homogenized solid, with material properties calculated from a representative volume element (RVE) of our structure of interest. The unit cell of the structure consists of carbon fiber framing supporting a Kapton membrane. Where relevant, we will calculate the material properties according to the weighted mean, for example in the case of certain moduli, or select the properties of the membrane when its properties are the limiting factor.

The material properties of this homogenized solid are transversely isotropic to emulate the orthotropy of a wound roll. Using cylindrical coordinates: E_θ, E_z, and $G_{z\theta}$ are defined by the in-plane properties of the structure of interest. The moduli that are directly affected by the coiling process are the radial modulus, E_R, and the shear moduli, G_{rz} and $G_{r\theta}$. E_R is dependent on the number of layers in the stack and increases the more tightly the coil is wound. The value of E_R must be found experimentally through compression testing, however here we will assume $E_r = 1\% E_\theta$, which is a typical order of magnitude result from stack compression experiments on wound roll materials [12].

The shear moduli G_{rz}, and $G_{r\theta}$ are properties that are directly impacted by our coiling tension stiffening scheme. As the coiling tension increases and the interlayer frictional shear capacity also increases, a measurable increase in

the shear stiffness of our coiled assembly should occur. A direct measurement of these values and correlation with winding tension and applied interlayer pressure is outside the scope of this study and is the topic for future research. For this FEA study, we will assume identical values of G_{rz} and $G_{r\theta}$ and, later in this paper, we will perform an indirect measurement by measuring the fundamental frequency of vibration. The material properties used in this simulation are found in Table 1.

Table 1 Homogenized Structure RVE Material Parameters

E_θ (GPa)	E_z (GPa)	E_R (GPa)	ν_{ij}	G_{ij} (GPa)	ρ_s (kg/m^3)
11.4	5.57	0.11	0.35	0.93	1600

B. FEA model setup and simulation procedure

We consider the configuration where the homogenized coiled structure is supported by an isotropic, aluminum mandrel, fixed in a cantilevered configuration. The mandrel is defined by the wall thickness t_m, length L, and outer radius r_m and is modeled using S4R shell elements. The coiled structure is defined by its thickness t_s and length L and is modeled using C3D20R solid elements. The structure is assumed to be perfectly bonded to the mandrel's outer diameter, but not to the mandrel's base, Fig. 3. The dimensions of the mandrel-coil system are shown in Table 2.

Table 2 Coiled Structure Geometry

r_m (m)	t_m (mm)	L (mm)	t_s (mm)
0.01	1	300	15

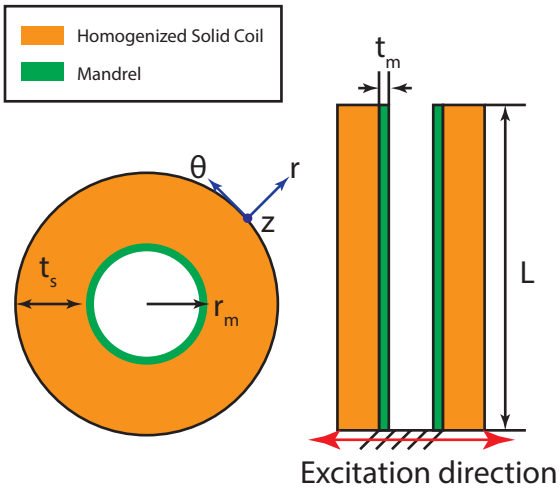

Fig. 3 Geometry of coiled structure.

The finite element software ABAQUS was used to estimate the location and loads for slip to occur in a coil under transverse vibration loading (Fig. 3). First, a linear frequency analysis (Lanczos solver) is performed on the assembly, extracting the first 10 modes. This model is then used in a modal dynamics step, where the transient response is determined using the extracted modes of the system as the basis. In the dynamics step, the structure is subjected to sinusoidal base excitation at the first natural frequency of the system in order to subject the assembly to the highest loads, using a span of acceleration levels from $1-15g$. Here 2% damping is assumed across all modes for the purpose of having a finite acceleration. The model is run for a duration sufficiently long for the maximum displacement of the structure to reach a steady state. The observed peak shear stress resultant for each acceleration level is compared against the shear capacity to determine the regions where slip would be expected.

C. Expected shear capacity due to winding

To determine the shear capacity of the coil using the winding model of interlayer stress, we will also homogenize the structure during the winding process. We will assume the sheet has a uniform thickness, h and is coiled with a constant winding stress equal to half the tensile yield stress of Kapton. We assume the coefficient of friction between layers corresponds to the Kapton-Kapton coefficient of friction. The assumed winding parameters are shown in Table 3. With these values, the interlayer stresses as a function of radial position in the coil are calculated according to Eq. 1 and the capacity is then found by scaling the result by the coefficient of friction as denoted in Eq. 2.

Table 3 Winding Parameters

Property	Value
Winding stress, $T_w = 0.5\sigma_{Y,Kapton}$	34.5 MPa
Structure thickness, h	0.05 mm
Number of layers, t_s/h	300
Coeff. friction, $\mu = \mu_{Kapton}$	0.48

The shear capacity as a function of the radial position is shown in Fig. 4. We observe that the the innermost layers are expected to have the largest shear capacity, and hence resistance to slip is largest at the mandrel-coil interface and reduces radially outward. This capacity must now be evaluated against the vibration induced shear stresses to determine the effectiveness of using friction to prevent interlayer slip.

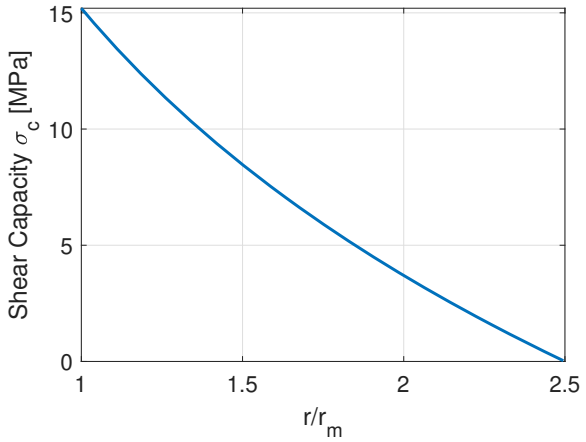

Fig. 4 Estimated shear capacity of coil wound with constant stress of 34.5 MPa.

D. Performance of coiled-stiff structure under vibration

The shear capacity of the coiled structure is compared to the maximum stress estimates from the FEA simulation to determine the load capacity of the coiled-stiff structure. The assembly's natural frequency is equal to the excitation frequency of 98.73 Hz. The stress components extracted from the vibration simulation are used to compute the stress resultant. The stress resultants for all layers are then consolidated into a histogram and plotted against the radial and axial position in the coil, shown in Fig. 5, to identify regions of high shear stresses. Superimposed on these plots is the maximum shear capacity at the corresponding radial or axial position. Note that the shear capacity varies radially and is invariant to axial position. Thus, in the axial direction, the maximum shear capacity curve is a constant.

From these plots, we observe that the maximum stresses are at the base of the structure, towards the mandrel interface. For magnitudes of excitation less than $5g$, no slip is expected anywhere. This result indicates load regions where modeling a coil as a homogenized solid may be considered a valid assumption. We note that the performance of the frictional capacity can be improved by either increasing the coiling tension or the coefficient of friction between layers.

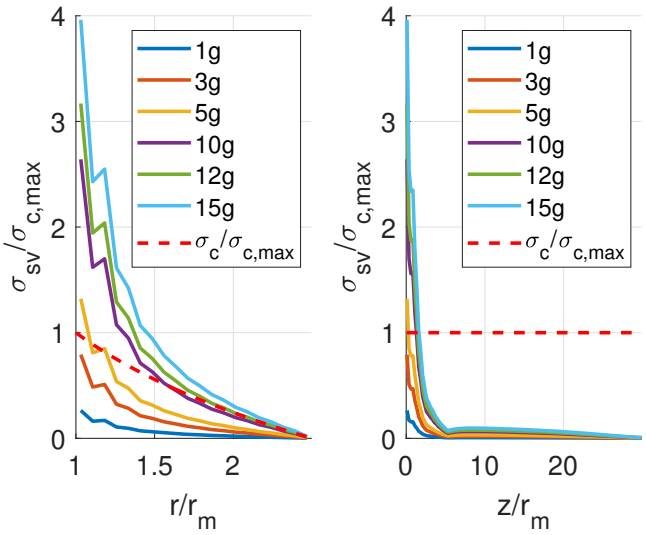

Fig. 5 Shear resultant histogram by location in the coil indicates that innermost layers towards the base of the coil are subject to highest vibration induced shear stresses.

A contour plot of the magnitude of the extracted stress components, normalized by the maximum shear capacity, is shown in Fig. 6 for the bottom-most layer of elements in the solid for 15g excitation. We observe that the highest stress is at the coil-mandrel interface. The out-of-plane axial shear σ_{RZ} is the largest (Fig. 6a), but has the same order of magnitude as $\sigma_{R\theta}$. Additionally, we see that the effect of $\sigma_{R\theta}$ extends for a larger radial distance in the coil, which indicates that a relatively large number of layers is affected by in-plane shear due to vibration loading (Fig. 6b). The FEA of the coiled-stiff model indicates that, despite having the highest interlayer stresses, and therefore the highest expected slip resistance, the innermost layers are the most important when considering slip. Therefore, for our initial experimental study, we will focus on the interlayer stresses at the mandrel interface.

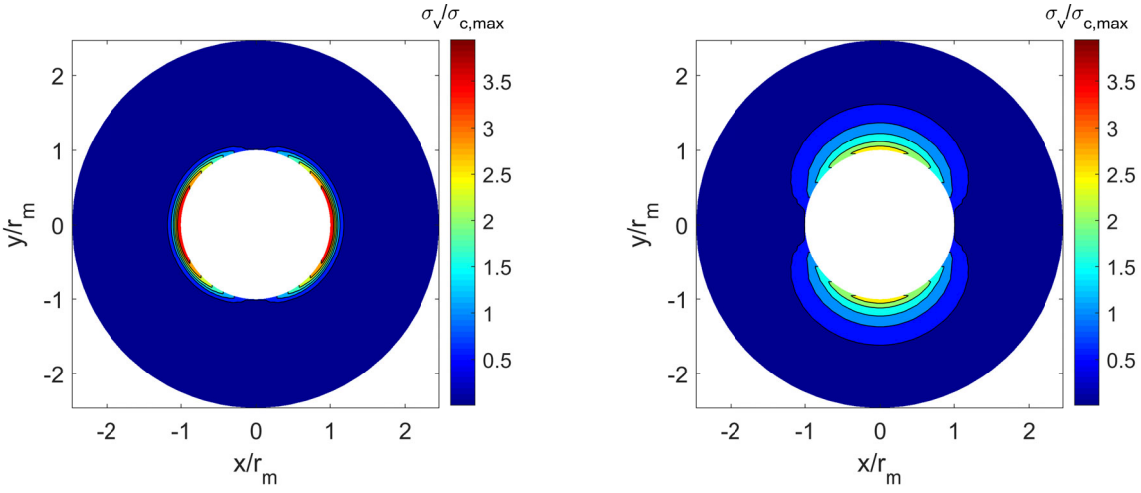

(a) Out of plane shear components σ_{RZ}. **(b) In plane shear components $\sigma_{R\theta}$.**

Fig. 6 Contour plots of stress components at the bottom of the coil due to 15g sinusoidal loading.

IV. Experimental Verification of Coiled-Stiff Concept

A. Fundamental frequency as a metric for shear stiffness of wound rolls

The utility of the vibration simulation results indicating regions and load levels where slip occurs is contingent upon the validity of the coiled-stiff model. In our simulation model, we assumed that our notional structure in the coiled configuration behaved as a solid with an assumed value of shear moduli, G_{rz} and $G_{r\theta}$, which are related to the tightness of the winding. Using these values, we were able to to obtain the fundamental frequency of our coiled structure for use in our loading cases. For an initial experimental study, we will evaluate the shear moduli indirectly using the fundamental frequency of the coil assembly. Here, fundamental frequency of the system is used as an indicator of whether the wound roll behaves as a solid under vibration. If the fundamental frequency of the coil system matches that of an equivalently sized solid, then our treatment of the roll as a continuous solid can be considered valid. We can measure how the apparent stiffness of the assembly varies with the coiling tension, focusing only on the pressure at the mandrel interface, which we indicated previously as the region where slip will initiate.

This experiment seeks to validate the following aspects of the coiled-stiff assumption:

1) Determine the effect of the coiling tension on the stiffness of the coiled assembly;
2) Study how this effect changes with excitation level.

B. Experiment design for sensitivity to coiling tension

For a small scale experimental study, we want a mandrel-coil assembly that is sensitive to coiling tension variation in order to provide the largest disparity in assembly stiffness between loosely and tightly coiled states, for a relatively small number of wound layers. Here a loosely coiled structure corresponds to a homogenized structure with low shear moduli G_{rz} and $G_{r\theta}$ and vice versa for a tightly coiled structure. Since we are not directly measuring the shear moduli, a range of values is considered up to the isotropic limit of Kapton: $G_{ij} = \frac{E}{2(1+\nu)}$. The disparity in stiffness, Δf is defined as the difference between the natural frequency corresponding to the minimum value of shear moduli required to have a bending mode, and the natural frequency obtained via shear moduli equal to the isotropic limit. For simplicity, the coiled material for this experiment was chosen to be 25 layers of continuous Kapton membrane, whose properties are shown in Table 4.

Table 4 Kapton Parameters

E_θ (GPa)	E_z (GPa)	E_R (GPa)	ν_{ij}	ρ_s (kg/m^3)	# Layers	h_{kapton} (mil)	t_s (mm)
4	4	0.4	0.35	1400	25	2	1.3

In order to design this experiment, the modal frequency extraction step of the coiled-stiff FEA model was reused to help choose a mandrel that would be most sensitive to changes in the winding tension of the selected membrane. A range of mandrel materials and geometries was considered and the most sensitive configuration corresponded to a mandrel with lower modulus and thinner wall. Choosing a mandrel of lower stiffness allows a limited number of windings to have a more pronounced effect. Additionally, we found that the disparity in stiffness increases with mandrel diameter. The significance of this result is that if the wound layers actually behave as a solid, the added layers from coiling effectively increase the overall thickness of the assembly, resulting in increased stiffness. This suggests that the stiffening effect associated with the coil-stiffened architecture scales with the size and stiffness of the structure being coiled. As a result of this design study, we fabricated a polycarbonate mandrel from stock material sized to fit the physical extents and measurement bandwidth of our test setup. The geometry and material property of the selected mandrel are presented in Table 5.

Table 5 Mandrel: FEA Analysis Parameters

r_m (mm)	t_m (mm)	L (mm)	E_m (GPa)	ρ_m (kg/m^3)
40	1.6	300	2.6	1200

Using the coiled-stiff FEA model for the selected experimental configuration, the expected disparity is approximately 45 Hz as shown in Fig. 7. We observe that for sufficiently large values of shear stiffness, i.e. coiling tension, the stiffness of the coil-mandrel assembly can exceed that of the mandrel alone. This demonstrates that the coiled membrane

provides stiffness to the system, rather than behaving as non-structural mass loading. If the coiled-stiff assumption is valid, we expect to see an increase in assembly stiffness with winding tension.

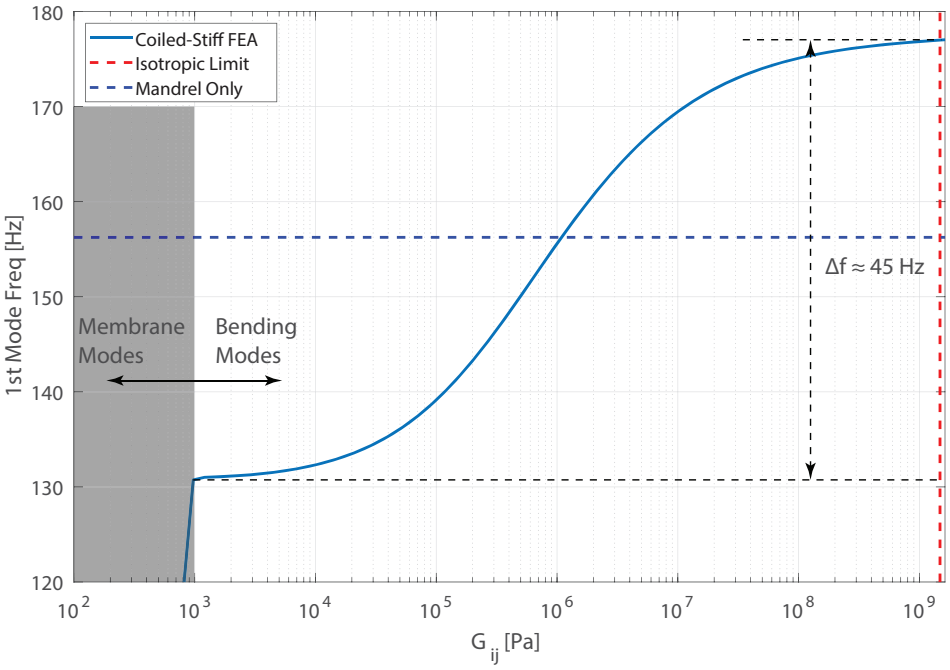

Fig. 7 Variation in stiffness with shear stiffness (coiling tension).

C. Sample winding procedure and interlayer stress measurement

A coiling apparatus that allows us to wind with varying tensions and a method of quantifying the interlayer stress applied are also needed. A constant tension winding machine was built to perform the winding-rewinding operation. The machine consists of a center wound mandrel with a current limited membrane roller, both driven by DC motors (Fig. 8). Kapton film is wound from the membrane roller onto the mandrel. At the start of winding, the first turn is attached to the mandrel via tape. At the end of winding, the free edge of the length of membrane is detached from the membrane roller and fixed to the coiled roll with tape.

The pre-stressed state of the roll after winding has terminated is measured using TekScan flexible A-201 100 lb range Force Sensitive Resistors (FSRs) inserted at the beginning of winding at the mandrel interface, under the first layer (Fig. 9). The FSRs are a pezioresistve element that converts force to voltage, which is read by a DAQ device. The FSRs have been calibrated using an Instron testing machine providing a mapping between measured voltage and applied load. Because the notional FEA results indicated that the stresses at the first winding layer are the most important, the results are only plotted against the stress measured by the FSR at the mandrel interface.

D. Experiment setup and procedure

The vibration experiment consists in shaking 25 layers of 2 mil thick Kapton®HN membrane, wound around a polycarbonate mandrel using our winding machine. The coiled roll is assembled using a range of different winding tensions, and parameterized by the interlayer stress measured at the innermost layer as measured using an FSR. The pre-loaded, coiled assembly is then placed on a vibration table, and retro-reflective tracking markers are placed in a grid arrangement on the outer layer as depicted in Fig.10. The tracking markers are used in concert with a Polytec PSV-500 Laser Scanning Vibrometer.

The vibrometer is used to control the vibration table, using random excitation for a range of excitation levels. The acceleration spectrum of the grid of tracker markers is recorded, and the averaged spectrum across all markers is evaluated. The fundamental frequency corresponds to the frequency of the first peak acceleration. For each tension level,

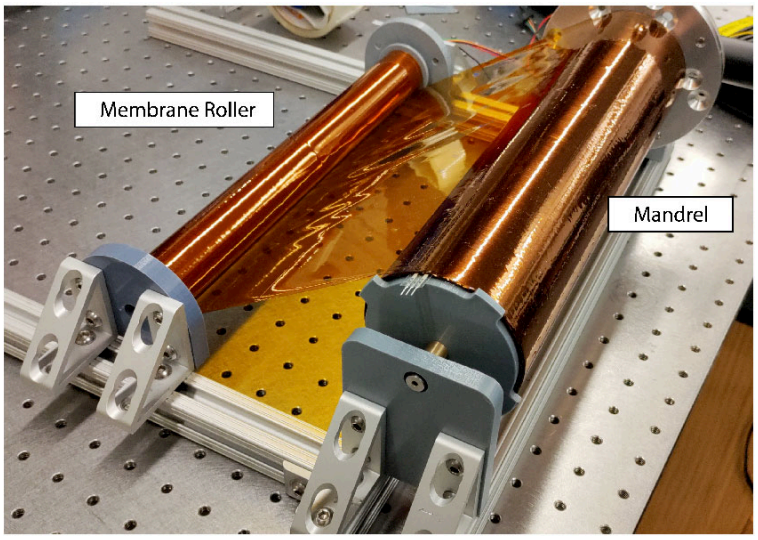

Fig. 8 Constant tension winding machine.

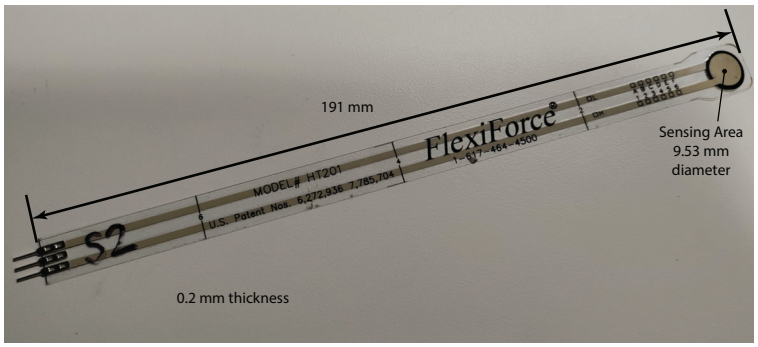

Fig. 9 Tekscan A-201 FSR Sensor.

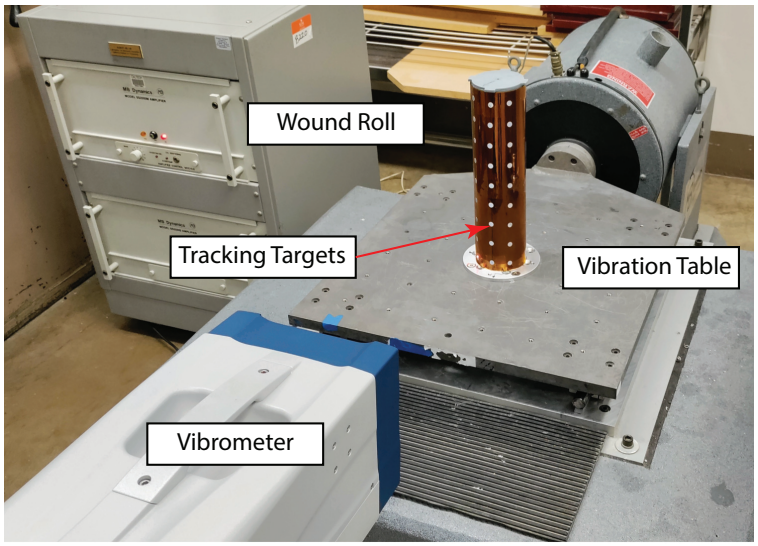

Fig. 10 Vibration experiment on a wound roll.

the scan at the lowest excitation level is repeated at the end of testing to ensure that no damage has occurred to the roll.

E. Results

The variation in the apparent stiffness of the wound roll with different winding tension has been measured. The fundamental frequency of the coil-mandrel assembly under different winding stresses as well as the mandrel by itself was recorded for a range of table excitation levels and is shown in Fig. 11. Superimposed on the figure, is the prediction from the coiled-stiff FEA model in green.

Looking at the mandrel only system, we note that the stiffness is approximately constant, irrespective of excitation level. This demonstrates that the mandrel fixture will provide a useful baseline comparison and any deviation in fundamental frequency results from the contribution of the wound roll. For the coil-mandrel assemblies, we observe that as the interface pressure increases, the assembly stiffness increases. Furthermore, the increase in stiffness is in line with the expected ranged predicted using the coiled-stiff FEA assumption, demonstrating the utility of this FEA model.

While the mandrel only stiffness was invariant with the excitation level, the coil-mandrel assembly system stiffness decreases with increasing acceleration. However, we also observe that increasing the interlayer pressure reduces this sensitivity to the excitation level. Despite the reduction in apparent stiffness under higher loads, the assemblies wound at higher tension maintain a higher fundamental frequency than the unloaded mandrel by itself, indicating that the windings provided some structural support. This is in contrast to the most loosely wound case, which behaved more like an added mass with the assembly stiffness decreasing below the mandrel-only level for sufficiently large acceleration.

The results of this experiment suggests that the simplification of treating a tightly wound roll as a continuous solid is a useful approximation, but its applicability may be limited beyond a critical load level. Better performance in this respect, may be achieved by increasing the winding tension or by increasing the coefficient of friction.

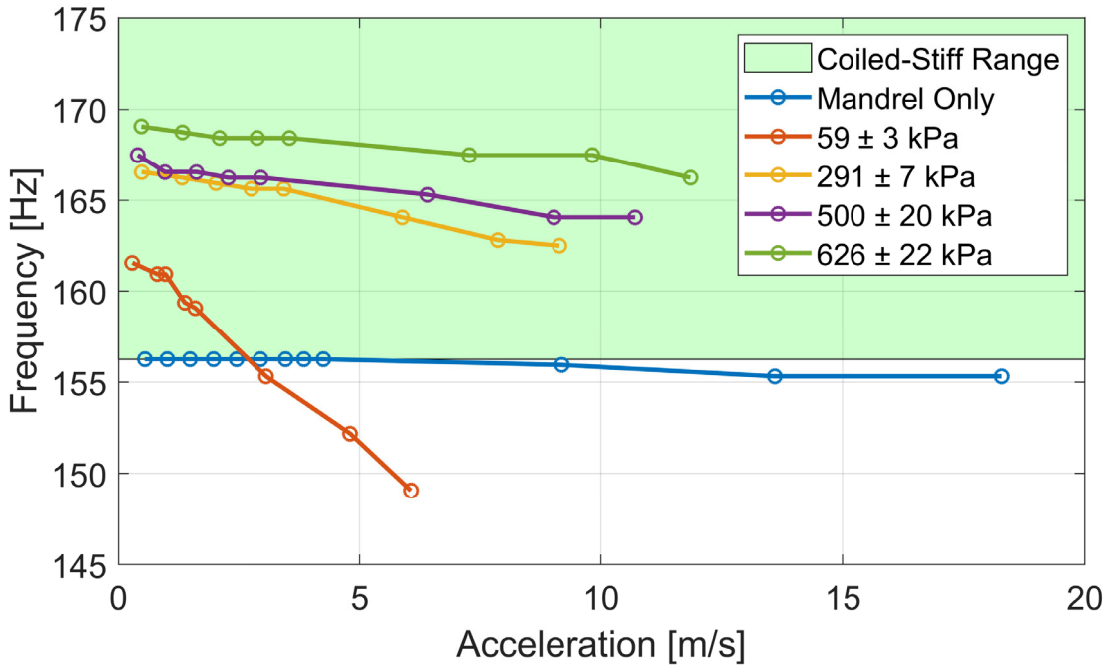

Fig. 11 Apparent stiffness of a pre-stressed, coiled assembly varies with preload.

V. Conclusion and Future Work

We have proposed a framework for estimating the slip resistance at any location in a tensioned, coiled structure using shear capacity estimates derived from the inter-layer stresses. Using an FEA model of a notional coiled structure supported by a cantilevered mandrel, the locations of maximum shear stresses in the structure are seen at the base, near the mandrel interface. Comparing the maximum shear resultant against the shear capacity indicates that for

some magnitudes of excitation, no slip is expected anywhere in the coil, indicating regimes where modeling a coil as a homogenized solid may be considered a valid assumption. The slip resistance of coil-stiffened structures can be increased either by increasing the winding tension, or by adjusting the inter-layer friction properties.

The utility of the coiled-stiff assumption was demonstrated using a simple vibration experiment on a roll of Kapton membrane wound around a mandrel. This experiment shows that the the coiled-stiff assumption can accurately predict the fundamental frequency of the coil assembly. Furthermore, it provides evidence in supporting the conjecture that increasing winding tension results in higher shear stiffnesses of the wound roll. The FEA study used to size this experiment also suggest that this stiffening effect scales with the size and stiffness of the coiled structure. As the structure becomes larger, the increasing number of wound layers increases the overall assembly thickness, thereby increasing the overall stiffness of assembly in the coiled configuration. This indicates potential for coilable structure architectures that rely on coiling pre-tension to provide integral packing and slip resistance, to scale with structure size.

Future experiments will explore the sensitivity of these results to interlayer friction, which is a factor of the shear capacity criterion that was not explored in this study. The coefficient of friction can be adjusted using traction modifiers, where we would expect an increase in friction to result in an increase in stiffness as measured by the fundamental frequency and vice versa. Direct measurement of the shear stiffness of pre-stressed layers, rather than the indirect method used in this study, will also be key to understanding the mechanics of tightly coiled structures. The applicability of this work in the future will be extended beyond simple continuous, homogenized sheets and extended to more realistic structures to determine if a frictional based method is capable of not only provided added stiffness to the system, but also prevent slip based defects in the packaged structure.

Acknowledgments

The authors acknowledge financial support from the Space Solar Power Project at Caltech.

References

[1] Okuizumi, N., Mori, O., Matsumoto, J., Saito, K., Sakamoto, H., Torisaka, A., and Shirasawa, Y., "Development of Deployment Structures and Mechanisms of Spinning Large Solar Power Sail," 2017.

[2] Carpenter, B., Banik, J., and Hausgen, P., "Roll-Out Solar Arrays (ROSA): Next Generation Flexible Solar Array Technology," 2017. doi:10.2514/6.2017-5307.

[3] Webb, D., Hirsch, B., Bradford, C., Steeves, J., Lisman, D., Shaklan, S., Bach, V., and Thomson, M., "Advances in starshade technology readiness for an exoplanet characterizing science mission in the 2020's," 2016, p. 99126H. doi:10.1117/12.2232587.

[4] Mori, O., Okuizumi, N., Chujo, T., and Takao, Y., "Improvement of sail storage and deployment mechanism for spin-type solar power sail," *Astrodynamics*, Vol. 4, No. 3, 2019, p. 223–231. doi:10.1007/s42064-019-0063-z.

[5] Webb, D., Hirsch, B., Bach, V., Sauder, J. F., Bradford, S., and Thomson, M., "Starshade Mechanical Architecture & Technology Effort," *3rd AIAA Spacecraft Structures Conference*, 2016. doi:10.2514/6.2016-2165.

[6] Changwoo, L., "Stresses and Defects in Roll Products: A Review of Stress Models and Control Techniques," *International Journal of Precision Engineering and Manufacturing*, Vol. 19, 2018, pp. 781–789. doi:10.1007/s12541-018-0094-z.

[7] Altmann, H., "Formulas for Computing Stresses in Center-Wound Rolls," *Tappi*, Vol. 51, No. 4, 1968, p. 176–179.

[8] Hakiel, Z., "Nonlinear Model For Wound Roll Stresses." *Tappi journal*, Vol. 70, 1987, pp. 113–117.

[9] Good, J. K., and Vaidyanathan, N., "Importance of torque capacity in predicting crepe wrinkles and starring in wound rolls," *International Conference on Web Handling*, 1995.

[10] Umali, J., Wilson, L., and Pellegrino, S., "Vibration Response of Ultralight Coilable Spacecraft Structures," 2017.

[11] Mollamahmutoglu, C., Adari, S., Bulut, O., and Good, J. K., "Coupling of winding models and roll quality instruments," *Proceedings of the 13th International Conference on Web Handling*, Oklahoma State University, 2015.

[12] Good, J., and Roisum, D., *Winding: Machines, Mechanics and Measurements*, TAPPI Press, 2008. URL `https://books.google.com/books?id=mg0Sdg8dCJwC`.